Charm dimuon production

Oleg Samoylov – *Dzhelepov Laboratory for Nuclear Problems, JINR, Dubna, Russia*

Abstract: We present our new measurement of charm dimuon production in neutrino-iron interactions based upon the full statistics collected by the NOMAD experiment. After background subtraction we observe 15,340 charm dimuon events, providing the largest sample currently available. The analysis exploits the large inclusive charged current sample (about 9 million events after all analysis cuts) to constrain the total systematic uncertainty to $\sim 2\%$. The extraction of strange sea and charm production parameters is also discussed.

Charm dimuon production in neutrino-nucleon interactions in the NOMAD experiment

R. Petti[1], O.B. Samoylov[2],
[1] University South Carolina, SC, USA
[2] Joint Institute for Nuclear Research, Dubna, Russia
e-mails: roberto.petti@cern.ch, samoylov@nusun.jinr.ru

Abstract

We present our new measurement of charm dimuon production in neutrino-iron interactions based upon the full statistics collected by the NOMAD experiment. After background subtraction we observe 15,340 charm dimuon events, providing the largest sample currently available. The analysis exploits the large inclusive charged current sample (about 9 million events after all analysis cuts) to constrain the total systematic uncertainty to $\sim$ 2%. The extraction of strange sea and charm production parameters is also discussed.

1 Introduction

Neutrino and anti-neutrino induced charm production can be used to extract the strange-quark parton distribution function (PDF) and to improve the knowledge about the transition to heavy quarks. In particular, the threshold behavior associated with the charm production is crucial for the extraction of $\sin^2\theta_{\rm W}$ from neutrino deep inelastic scattering (DIS) data. Furthermore, a better understanding of the inclusive charm production cross-section is important for the background determination of the experiments aiming at the study of neutrino oscillations.

In the case of muon neutrino scattering, the underlying process is a neutrino charged-current (CC) interaction with a s- or d-quark, producing a c-quark that fragments into a charmed hadron. The charmed hadron may decay semi-leptonically producing opposite sign dimuons through the process shown in Fig. 1.

Similarly, a muon anti-neutrino can interact with a $\bar{\rm s}$- or $\overline{\rm d}$-quark, producing a $\bar{\rm c}$-quark that fragments into a charmed hadron, again leading to a final state with two oppositely charged muons.

2 Cross-section for charm dimuon production

In the first approximation, the charm production double differential cross-section by neutrino deep inelastic scattering assuming an isoscalar target, massive charm quark slow rescaling $\xi = x + m_{\rm c}^2/2M\nu$ [1], the Callan-Gross relationship [1] and limit that $Q^2 \gg M^2$ is

$$\frac{d^2\sigma_{\rm c}^{\nu}}{d\xi dy} = \frac{G_{\rm F}^2 M E_{\nu}}{\pi}\left(\frac{M_{\rm W}^2}{M_{\rm W}^2+Q^2}\right)^2\left[|V_{\rm cs}|^2\xi s(\xi,Q) + |V_{\rm cd}|^2\xi\frac{u(\xi,Q)+d(\xi,Q)}{2}\right], \qquad (1)$$

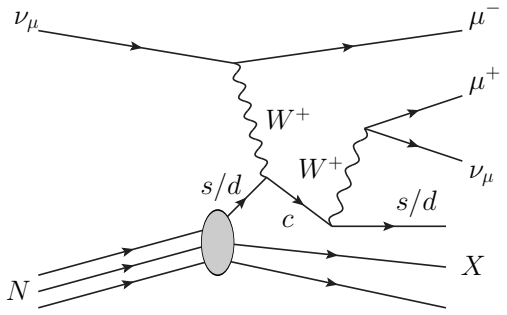

Figure 1: *Neutrino induced charm dimuons.*

where E_ν, x, y, ν, Q are standard DIS quantities, G_F is the Fermi constant, M_W is the W-boson mass, M is the proton mass, V_cs, V_cd are the Cabibbo-Kobayashi-Maskawa (CKM) matrix elements, $u(x)$, $d(x)$, $s(x)$ are the parton densities of the up, down and strange quarks.

The fragmentation process describes the recombination of the charm quark with an anti-quark from the nucleon sea. It is conventionally represented by a fragmentation function $D(z)$, which specifies the probability that a given charmed hadron will carry a fraction z of the momentum of the initial c-quark. In the quark parton model (QPM) [1] the fragmentation function is factorized from double differential cross-section for c-quark production. This is not true in higher order quantum chromodynamics (QCD) theory.

The final double differential cross-section for dimuon production at leading order in QCD is

$$\frac{d^2\sigma^\nu_{\mu\mu}}{d\xi dy} = \frac{d^2\sigma^\nu_\mathrm{c}}{d\xi dy} D(z) B_\mu, \tag{2}$$

where the factor $B_\mu \equiv B_\mathrm{c}(\mathrm{c} \to \mu^+\nu_\mu\mathrm{X})$ is the probability that the charmed hadron will decay semi-muonically.

From the charm dimuon double differential cross-section we can conclude:

1. The CKM matrix element $|V_\mathrm{cd}|^2$ is much smaller than $|V_\mathrm{cs}|^2$ (0.0507 as opposed to 0.9476). Therefore the (anti)neutrino induced dimuon x_Bj distributions are sensitive to the shape of strange quark momentum distributions, providing a means for the extraction of the strange quark density.

2. The slow rescaling mechanism naturally includes the mass of the c-quark. The visible neutrino energy E_ν and the partonic center-of-mass energy squared $\hat{s} = Q^2(1/x-1)$ distributions should be sensitive to this mass.

The current knowledge of the strange sea content of the nucleon in the global PDF fits is based on the NuTeV and CCFR dimuon data [2]. The table 1 summarises the available relevant neutrino dimuon data samples.

Exp.	Publ.	Stat. ($N_{\mu\mu}$)	E_ν (GeV)
CDHS	1982 [3]	9,922	30-250 (20)
CHARM II	1999 [4]	3,100	35-300 (24)
CCFR	2001 [5, 6]	5,030	30-600 (150)
NuTeV	2001 [6]	5,102	20-400 (157.8)
CHORUS	2008 [7]	8,910	15-240 (27)
NOMAD	2011	15,340	6-300 (27)

Table 1: *Summary of existing measurements of charm dimuons in neutrino interactions. The NOMAD analysis described in this paper has the largest statistics and the lowest energy threshold.*

3 The NOMAD detector

The largest sample of neutrino interactions, about 9 millions, measured in NOMAD together with the excellent reconstruction quality of muon tracks and the good calorimetry, offer an excellent opportunity to study neutrino induced charm dimuon production. The NOMAD detector [8] consisted of an iron-scintillator front calorimeter (FCAL) with a total mass of 17.7 tons (5 nuclear interaction lengths deep) and an active target of 44 drift chambers (DCH), with a total fiducial mass of 2.7 tons, located in a 0.4 T dipole magnetic field, as shown in Fig. 2. The neutrinos are primarily produced by the

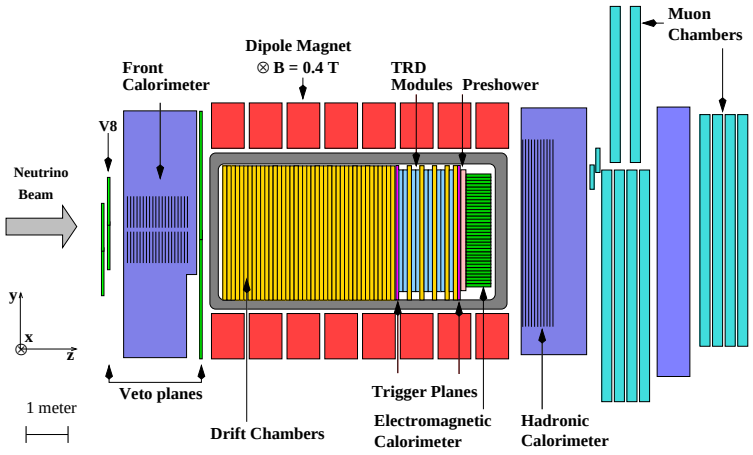

Figure 2: *Side view of the NOMAD detector*

decay in flight of π/K mesons produced by beam of 450 GeV protons incident on a beryllium target. Relative abundance of the beam composition is $\nu_\mu : \overline{\nu}_\mu : \nu_\mathrm{e} : \overline{\nu}_\mathrm{e} = 1.0 : 0.0678 : 0.0102 : 0.0027$ [9].

3.1 The front calorimeter

FCAL consists of 23 iron plates which are 4.9 cm thick and separated by 1.8 cm gaps. Twenty out of the 22 gaps are instrumented with long scintillators which are read out on both ends by 3 in photomultipliers. The dimensions of the scintillators are $175 \times 18.5 \times 0.6$ cm^3. To achieve optimal light collection and a reasonable number of electronic channels five consecutive scintillators along the beam axis are ganged together by means of twisted light guides and form a module. Ten such modules are placed above each other and form a stack. Along the beam axis are four stacks. The area of the FCAL "seen" by the neutrino beam is 175×190 cm^2.

3.2 The Monte Carlo simulation

The NOMAD Monte Carlo simulation (MC) is based on LEPTO 6.1 [10] and JETSET 7.4 [11] generators for neutrino interactions, and on a GEANT [12] based program for the detector response. The default LEPTO cross-sections defines the parton content of the nucleon for the cross-section calculation in the LO approximation with GRV94 PDFs [13]. In Sec. 6.1 described modification of the cross-section calculation using in present analysis.

4 Event selection

We select two types of interactions: the inclusive CC neutrino interactions on iron (single muon) and the opposite sign dimuons in CC interactions (two muons). The main selection cuts are the following:

1. FCAL trigger;
2. One reconstructed and identified μ^-;
3. Fiducial volume inside the sensitive region of FCAL;
4. A second reconstructed μ^+ (from c-quark production or backgrounds) or μ^- (from backgrounds);
5. Time difference between the two muons less than 5 ns to reject backgrounds;
6. Leading negative muon requirement to reject anti-neutrino background: the transverse momentum of the current muon, $P^{\mathrm{T}}_{\mu_{\mathrm{cc}}}$, larger than the transverse momentum of the secondary muon, $P^{\mathrm{T}}_{\mu_{\mathrm{c}}}$;
7. Visible hadronic FCAL energy less than 100 GeV and total visible neutrino energy less than 300 GeV;
8. Energy of the current muon greater than 3 GeV;
9. Energy of the secondary muon (or the visible hadronic energy for CC) larger than 3 GeV;
10. Four-momentum transfer squared Q^2 greater than 1 GeV^2/c^2.

The cuts 4–7 are relevant for the dimuon sample only. All the applied cuts are relatively loose in order to reduce systematic uncertainties. The main goal of the selection is to ensure that the events are well measured in FCAL. We limit our analysis to the region $Q^2 > 1$ GeV^2/c^2 in which we can reliably calculate the cross-sections within the parton model. It must be also noted that the impact of such cut on the charm sample is negligible, due to the intrinsic production threshold.

5 Background subtraction

An event is assumed to be a ν_μ CC event in the presence of reconstructed and identified negative muon track. The background become from the ν_μ neutral current (NC) events in which one of hadrons decays in flight with μ^- production or ν_e, $\overline{\nu}_\mu$, $\overline{\nu}_\mathrm{e}$ events where a lepton was identified as a muon. The ν_μ CC background was estimated from simulation to be less than 0.5%.

The charm dimuon events are determined from the opposite sign dimuons (OSDM) measured in the data after subtracting the background originated from the muonic decay of π^+ and K^+ mesons:

$$N^{\mathrm{DATA}}_{\mu\mu_\mathrm{c}} = N^{\mathrm{DATA}}_{\mu\mu^+} - N^{\mathrm{DATA}}_{\mu\mu^+_\mathrm{bg}} \tag{3}$$

The background events $N^{\mathrm{DATA}}_{\mu\mu^+_\mathrm{bg}}$ are estimated from the like sign dimuons (LSDM) measured in the data ($\mu^-\mu^-$), multiplied by a scale factor extracted from the MC:

$$N^{\mathrm{DATA}}_{\mu\mu^+_\mathrm{bg}} = N^{\mathrm{DATA}}_{\mu\mu^-} \cdot \left(N^{\mathrm{MC}}_{\mu\mu^+_\mathrm{bg}} / N^{\mathrm{MC}}_{\mu\mu^-} \right) \tag{4}$$

where the scale factor is given by the ratio of opposite sign to like sign dimuon events originated from meson decays.

Figure 3 shows the distributions of the LSDM events in FCAL data and MC. The general agreement is satisfactory since we note the LSDM event from MC are never directly used in our analysis. Rather, we only use the ratio of OSDM to LSDM background events in MC. This ratio is very sensitive to the details of the fragmentation of the hadronic system, in particular at low momenta. For this reason we cannot rely on the MC at the level of precision of a few percent. Instead, we follow a different approach. The background scale is basically determined by the ratio of positively charged to negatively charged mesons inside the hadronic system produced by the fragmentation of partons in DIS events. Therefore, we measure this latter ratio as a function of the meson momentum from the NOMAD data originated in the light Drift Chamber target (DCH). The difference between target nuclei (carbon in DCH vs. iron in FCAL) turns out to be negligible for the inclusive fragmentation variables from a direct comparison between the corresponding MC samples.

After measuring the ratio of positively charged to negatively charged mesons from DCH data, we re-weight each positive meson originated from the hadronic system in FCAL events according to the measured ratio ω_{h^+}:

$$W^{\mathrm{MC}} = \prod_{\mathrm{h}^+} \omega_{\mathrm{h}^+} \tag{5}$$

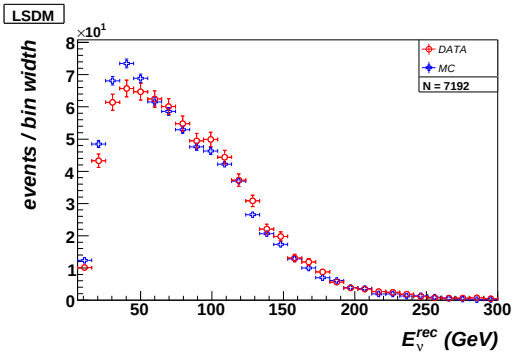

Figure 3: *Distributions of the reconstructed visible neutrino energy in like-sign dimuon events. Data are shown as circles while MC points are shown as crosses.*

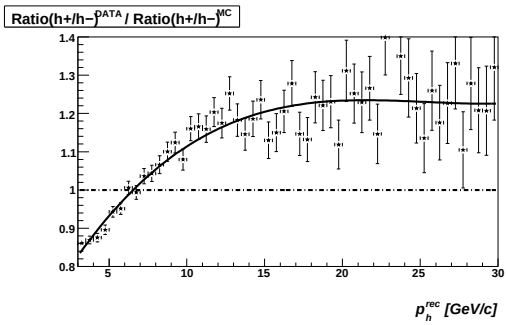

Figure 4: *Double ratio between positively charged and negatively charged mesons h^+/h^- in DCH data and MC as a function of their momentum.*

As a result, the entire background estimate for the charm dimuon sample is based upon data themselves, which are used both for the LSDM and for the background scale. Figure 4 shows the measured ratio h^+/h^- from the DCH data, as well as a comparison with the corresponding MC simulation. The calibration of the background through the re-weighting procedure is a crucial step in the analysis and allows a substantial improvement in the description of the charm dimuon data by the MC. Without the use of data from the low density DCH target it would have not been possible to lower the energy threshold on the secondary muon to 3 GeV as well as to reduce the systematic uncertainty on the background subtraction.

6 The cross-section measurement

After the background subtraction we have 15,340 neutrino induced charm dimuon events and about 9 million inclusive charged current events shown in Fig. 5.

We measure the ratio of the charm dimuon cross-section to the inclusive CC cross-section, as a function of the kinematic variables:

$$\mathcal{R}_{\mu\mu}(x) \equiv \sigma_{\mu\mu}/\sigma_{\rm cc} \simeq N_{\mu\mu}/N_{\rm cc}(x), \text{ where } x = E_\nu, x_{\rm Bj}, \sqrt{\hat{s}} \tag{6}$$

The ratio $\mathcal{R}_{\mu\mu}$ provides a large cancellation of all systematic uncertainties affecting both the numerator and the denominator. Moreover, the energy dependence of the rate provides information on the charm mass.

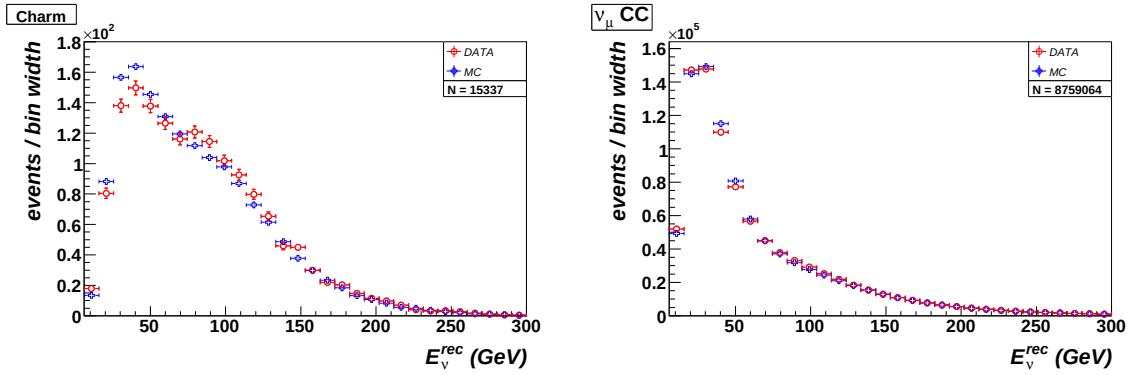

Figure 5: *Distributions of the reconstructed visible neutrino energy in charm dimuon (left) and inclusive CC (right) events. Data are shown as circles while MC points are shown as crosses.*

6.1 Cross-section weights

The MC events used in the analysis were produced with the default LEPTO cross-sections, which for the DIS are calculated in the LO approximation with GRV94 PDFs [13]. This simulation does not adequately describe the charm production process since it does not include any rescaling mechanism to take into account the large mass of the charm quark. Furthermore, no electroweak, nuclear and high twist corrections are included.

In order to achieve an accurate description of data, we implement a re-weighting procedure for the charm cross-section:

$$\omega_{\mu\mu}(E_\nu, x_{\rm Bj}, y_{\rm Bj}) = \frac{\sigma^{\rm AKP}_{\mu\mu}(E_\nu, x_{\rm Bj}, y_{\rm Bj})}{\sigma^{\rm LEPTO}_{\mu\mu}(E_\nu, x_{\rm Bj}, y_{\rm Bj})} \tag{7}$$

where $\sigma^{\rm LEPTO}_{\mu\mu}$ is the original LEPTO cross-section used to generate the MC events and $\sigma^{\rm AKP}_{\mu\mu}$ is the new cross-section obtained from an analytical calculation [2, 14, 15, 16, 17]. The charm cross-section is calculated in the NLO QCD approximation for the heavy quark structure functions, in a factorization scheme with 3 light flavors in the initial state (FFS) [2]. The Target Mass Corrections (TMC) are implemented following the prescription by Georgi and Politzer [18]. The impact of the dynamical High Twist corrections to the charm production is evaluated by applying a simple rescaling for the quark charge to the phenomenological twist-4 terms extracted from the inclusive lepton-nucleon cross-sections [14]. We apply nuclear corrections using the calculations of Refs. [15, 16]. This calculation takes into account a number of different effects including the Fermi motion and binding, neutron excess, nuclear shadowing. nuclear pion excess and the off-shell correction to bound nucleon SFs. The electroweak corrections, including one-loop terms, are calculated according to Ref. [17] within the framework of the parton model. The parameters related to charm production like the mass of the charm quark and the strange sea distribution are fixed to the ones extracted from the global PDF fit including NuTeV and CCFR charm dimuon data [2] at this stage. This

allows a consistency check with a calculation fully independent from NOMAD data.

Finally, we apply an additional re-weighting to the charm events to take into account the effect of the charm fragmentation, which is described by the Collins-Spiller function. This function describes the probability for a charmed hadron to carry a given fraction $z = P^{\mathrm{L}}(h_{\mathrm{c}})/P^{\mathrm{L}}_{\mathrm{max}}$ of the longitudinal momentum and is defined by one free parameter ε.

Another additional thing we apply to the charm dimuon events to take into account the effect of the semi-leptonic branching ratio B_μ as a function of the neutrino energy from a fit to the E531 data described in [2]:

$$B_\mu(E_\nu) = \frac{0.0950}{1 + 6.898/E_\nu} \tag{8}$$

We apply a similar re-weighting procedure to the inclusive ν_μ CC events (single muons). The model used for the inclusive CC structure functions on iron is the same described above for the charm production. The light quark contributions to the SFs are calculated in the NNLO QCD approximation. Figure 5 shows comparisons between data and weighted MC for the reconstructed visible neutrino energy in charm dimuon and inclusive ν_μ CC events.

6.2 The unfolding

After re-weighting of the MC events to our cross-section model, we unfold the detector response from the measured data for both the inclusive ν_μ CC and the charm dimuon events. To do this the first determine the smearing matrix and the efficiency corrections from the MC simulation:

$$N_i^{\mathrm{rec}}(x^{\mathrm{rec}}) = \sum_j r_{ij}(x^{\mathrm{rec}}, x^{\mathrm{sim}}) \times \epsilon_j(x^{\mathrm{sim}}) \times N_j^{\mathrm{sim}}(x^{\mathrm{sim}}) \tag{9}$$

where x^{rec} and x^{sim} are the reconstructed and simulated variable x ($x = E_\nu, x_{\mathrm{Bj}}, \sqrt{\hat{s}}$). The inverse of the above relation provides the unfolded measurement:

$$N_j^{\mathrm{sim}}(x^{\mathrm{sim}}) = \sum_i \epsilon_i^{-1}(x^{\mathrm{sim}}) \times r_{ji}^{-1}(x^{\mathrm{sim}}, x^{\mathrm{rec}}) \times N_i^{\mathrm{rec}}(x^{\mathrm{rec}}). \tag{10}$$

The binning of the data points is performed in such a way that the bin size is comparable to the experimental resolution in order to reduce the impact of non-diagonal terms in the smearing matrix.

We validate the unfolding procedure by splitting the available MC events in two independent samples. The first sample (biased) is used to extract the smearing matrix and the efficiency correction. The second half of the MC sample (unbiased) is used as fake data to determine the unfolded distributions. These latter are then compared with the input simulated variables of the unbiased sample. This procedure can reproduce the input distributions in the unbiased sample with a good accuracy for both ν_μ CC and charm dimuon events. Finally we compare the unfolded distributions obtained from FCAL data and MC with an analytical calculation performed by convolution our cross-section model with the neutrino flux. The results are shown in Figures 6.

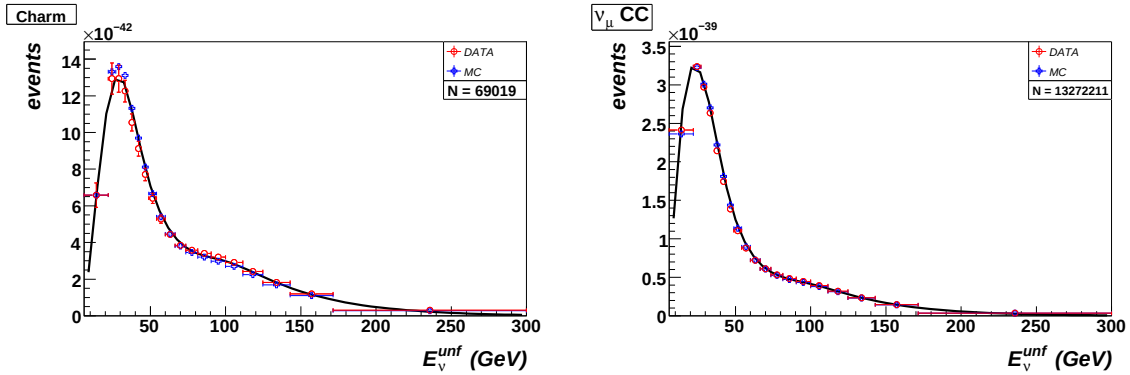

Figure 6: *Distributions of the unfolded neutrino energy in charm dimuon (left) and inclusive CC (right) events. Data are shown as circles while MC points are shown as crosses. The curves is analytical model calculations.*

6.3 Systematic uncertainties

For the experimental systematic uncertainties we consider the variation of all analysis cuts, the muon and hadron energy scales and the flux prediction. For the model systematic uncertainties we take into account the following sources: the background scale factor, the charm fragmentation, the mass of charm quark, uncertainties on structure functions including strange sea, high twists, electroweak and nuclear corrections. Overall we include 17 different sources of systematic uncertainties. It must be noted that he ratio $\mathcal{R}_{\mu\mu}$ provides a large cancellation of all the systematic uncertainties affecting both the numerator and the denominator. Therefore, the dominant systematic uncertainties are the contributions related specifically to the extraction of the charm production signal (the numerator): the background scale factor, the charm fragmentation and the mass of c-quark. The total systematic uncertainty on $\mathcal{R}_{\mu\mu}$ turns out to be around 2%. Both statistical and systematic uncertainties are shown in Fig. 7.

7 Results

In Fig. 7 we present the final ratio $\mathcal{R}_{\mu\mu}$ between charm dimuon cross-section and inclusive ν_μ CC cross-section, as a function of the visible neutrino energy. Both statistical and systematic uncertainties are shown and a bin centering correction has been applied. The solid curves represent the result of an analytical calculation fully independent from NOMAD data and based upon our cross-section model. A comparison with previous measurements is also given for completeness.

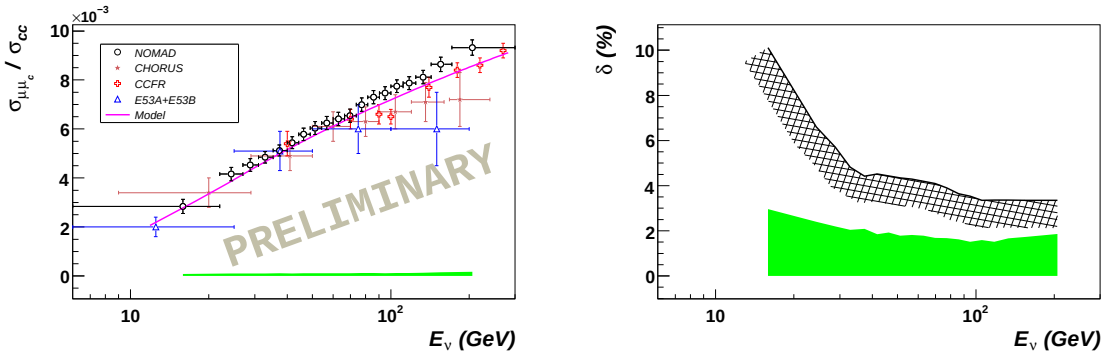

Figure 7: *Final ratio $\mathcal{R}_{\mu\mu}$ between charm dimuon cross-section and inclusive ν_μ CC cross-section as a function of the visible neutrino energy (left). The right plots give the relative statistical (black curve) and systematic (the band) uncertainties in percentage.*

8 Summary

We performed our study of charm dimuon production in neutrino-iron interactions based upon the full statistics collected in FCAL by the NOMAD experiment. After background subtraction we observe 15,340 charm dimuon events, providing the largest sample currently available. The analysis exploits the large inclusive charged current sample (about 9 million events after all analysis cuts) to constrain the total systematic uncertainty to $\sim 2\%$. This result will be extended soon with $x_{\rm Bj}$ and $\sqrt{\hat{s}}$ distributions, allowing an improvement in the knowledge of the strange sea content of the nucleon and of the charm mass by more than a factor of 2 with respect to previous determinations.

Acknowledgement

We gratefully acknowledge the CERN SPS accelerator and beam-line staff for the magnificent performance of the neutrino beam. The experiment was supported by the following funding agencies: Australian Research Council (ARC) and Department of Education, Science, and Training (DEST), Australia; Institut National de Physique Nucléaire et Physique des Particules (IN2P3), Commissariat à l'Energie Atomique (CEA), France; Bundesministerium f̈ur Bildung und Forschung (BMBF, contract 05 6DO52), Germany; Istituto Nazionale di Fisica Nucleare (INFN), Italy; Joint Institute for Nuclear Research (JINR) and Institute for Nuclear Research of the Russian Academy of Sciences, Russia; Fonds National Suisse de la Recherche Scientifique, Switzerland; Department of Energy, National Science Foundation (grant PHY-9526278), the Sloan and the Cottrell Foundations, USA. The special supports for this analysis have got from NOMAD CERN fund, Switzerland; Istituto Nazionale di Fisica Nucleare (INFN), Sezione di Pisa, Italy; Joint Institute for Nuclear Research (JINR, grant for junior scientific researchers, 2009), Russian Foundation for Basic Research (RFBR, grant 10-02-00395-a), Russian Federal Targeted Program "Research and Research-Human Resources for Innovating Russia" (contract 02.740.11.5220), Russia.

We also thank L. Di Lella, L. Camilleri, V. Cavasinni, S. Alekhin and D. Naumov for valuable discussions.

Bibliography

[1] *Nakamura K. et al. (Particle Data Group).* Review of particle physics. // J. Phys. G. 2010 V. 37. 075021.

[2] *Alekhin S., Kulagin S. A. and Petti R.* Determination of Strange Sea Distributions from Neutrino-Nucleon Deep Inelastic Scattering. // Phys. Lett. B. 2009. V. 675. P. 433–440; arXiv:0812.4448 [hep-ph].

[3] *Abramowicz H. et al.* Experimental Study Of Opposite Sign Dimuons Produced In Neutrino And Anti-Neutrinos Interactions. // Z. Phys. C. 1982. V. 15. P. 19–31.

[4] *Vilain P. et al.* Leading-order QCD analysis of neutrino induced dimuon events. // Eur. Phys. J. C. 1999. V. 11. P. 19–34.

[5] *Bazarko A. O. et al. (CCFR Collaboration).* Determination Of The Strange Quark Content Of The Nucleon From A Next-To-Leading Order QCD Analysis Of Neutrino Charm Production. // Z. Phys. C. 1995. V. 65, No. 2. P. 189–198; arXiv:hep-ex/9406007.

[6] *Goncharov M. et al. (NuTeV Collaboration).* Precise measurement of dimuon production cross-sections in nu/mu Fe and anti-nu/mu Fe deep inelastic scattering at the Tevatron. // Phys. Rev. D. 2001. V. 64. 112006; arXiv:hep-ex/0102049.

[7] *Kayis-Topaksu A. et al. (CHORUS Collaboration).* Leading order analysis of neutrino induced dimuon events in the CHORUS experiment. // Nucl. Phys. B. 2008. V. 798. P. 1–16; arXiv:0804.1869 [hep-ex].

[8] *Altegoer J. et al. (NOMAD Collaboration).* The NOMAD experiment at the CERN SPS. // Nucl. Instrum. Meth. A. 1998. V. 404. P. 96–128.

[9] *Astier P. et al. (NOMAD Collaboration).* Prediction of neutrino fluxes in the NOMAD experiment. // Nucl. Instrum. Meth. A. 2003. V. 515. P. 800–828; arXiv:hep-ex/0306022.

[10] *Ingelman G.* LEPTO version 6.1: The Lund Monte Carlo for deep inelastic lepto - nucleon scattering. // Proceedings of Workshop on Physics at HERA. Hamburg, Germany, 29-30 Oct 1991. P. 1366–1394.

[11] *Sjostrand T.* High-energy physics event generation with PYTHIA 5.7 and JETSET 7.4. // Comput. Phys. Commun. 1994. V. 82. P. 74–90.

[12] *Brun R., Carminati F. and Giani S.* GEANT Detector Description and Simulation Tool. CERN-W5013. Oct 1994. 430pp.

[13] *Gluck M. et al.* Next-to-leading order radiative parton model analysis of polarized deep inelastic lepton - nucleon scattering. // Phys. Rev. D. 1996. V. 53. P. 4775–4786; arXiv:hep-ph/9508347.

[14] *Alekhin S., Kulagin S. A. and Petti R.* Modeling Lepton-Nucleon Inelastic Scattering from High to Low Momentum Transfer. // AIP Conf. Proc. 2007. V. 967. P. 215–224; arXiv:0710.0124 [hep-ph].

[15] *Kulagin S. A. and Petti R.* Neutrino inelastic scattering off nuclei. // Phys. Rev. D. 2007. V. 76. 094023; arXiv:hep-ph/0703033.

[16] *Kulagin S. A. and Petti R.* Global study of nuclear structure functions. // Nucl. Phys. A. 2006. V. 765. P. 126–187; arXiv:hep-ph/0412425.

[17] *Arbuzov A. B., Bardin D. Y. and Kalinovskaya L. V.* Radiative corrections to neutrino deep inelastic scattering revisited. // JHEP. 2005. V. 0506. 078; arXiv:hep-ph/0407203.

[18] *Georgi H. and Politzer H. D.* Freedom At Moderate Energies: Masses In Color Dynamics. // Phys. Rev. D. 1976. V. 14. P. 1829–1848.